Chiral Discrimination in the Gas Phase Using Different Transducers: Thickness Shear Mode Resonators and Reflectometric Interference Spectroscopy

ARTICLE *in* ANALYTICAL CHEMISTRY · AUGUST 1997

Impact Factor: 5.64 · DOI: 10.1021/ac9612990 · Source: PubMed

7 AUTHORS, INCLUDING:

Andreas Hierlemann
ETH Zurich
290 PUBLICATIONS **4,834** CITATIONS
SEE PROFILE

Günter Gauglitz
University of Tuebingen
350 PUBLICATIONS **9,011** CITATIONS
SEE PROFILE

Anal. Chem. **1997,** *69,* 3058−3068

Chiral Discrimination in the Gas Phase Using Different Transducers: Thickness Shear Mode Resonators and Reflectometric Interference Spectroscopy

K. Bodenhöfer,[†] A. Hierlemann,*[,†] J. Seemann,[†] G. Gauglitz,[†] B. Christian,[‡] B. Koppenhoefer,[‡] and W. Göpel[†]

Center of Interface Analysis and Sensors, and Institute of Physical and Theoretical Chemistry, Institute of Organic Chemistry, University of Tübingen, Auf der Morgenstelle 8, D-72076 Tübingen, Germany

The discrimination of optical isomers (enantiomers) in the gas phase has been performed using two different analytical tools: thickness shear mode resonators (TSMRs) and reflectometric interference spectroscopy (RIFS). The selective coatings included both enantiomers ((*S*)- and (*R*)-receptor) of a Chirasil-Val derivative (stationary phase material in GC) with octyl side chains. Successful discrimination of the enantiomers of different types of analytes (amino acids and lactates) was achieved. The results of both transduction methods were consistent and in good agreement with GC measurements. In addition, different mixtures of both enantiomers of the respective analyte were measured, and the enantiomeric composition could be quantitatively determined with excellent reliability. Since the sensors allow on-line monitoring (not possible with GC) of enantiomeric purity, an application in industrial synthesis (process control) of such compounds represents an interesting feature, especially with regard to the tested derivatives of lactic acid.

The discrimination of chiral antipodes is considered to be one of the most difficult tasks in analytical chemistry, since the physical and chemical properties of enantiomers are identical in a nonchiral environment. Hence, chiral recognition structures have to be employed to perform a successful recognition of the respective enantiomer or to determine the enantiomeric purity/enantiomeric composition of a certain compound. Especially in medical applications, this is very important, since in several cases only one of the enantiomers contributes to the desired pharmaceutical effect (e.g., anesthetics[1]) or, even worse, is toxic or teratogenic (thalidomide[2]). The human nose is able to discriminate only few pairs of enantiomers, e.g., different smells of the enantiomers of rose oxide[3] or limonene.

For many years, discrimination of optical isomers (enantiomers) has been achieved in gas chromatography (GC) by using mainly three different types of stationary phase materials: (i) *coordination* of the optically active compound *to metal*-chelate-containing polysiloxanes (see, e.g., ref 4); (ii) intramolecular *entrapment* performed *by cavities* such as cyclodextrins, (cyclic oligomeric polysaccharides), as presented in, e.g., refs 5 and 6; and (iii) the recognition of enantiomeric analytes by chiral amide stationary phases based mainly on *hydrogen bonding* as described in refs 7 and 8.

The advantage of GC analysis is that both enantiomers can be detected simultaneously on the same stationary phase, and the enantiomeric purity and excess can be determined by comparing the signals (peak areas) of both antipodes. An important drawback is that GC is an off-line procedure, and hence an on-line control of industrial processes is not possible. Here is a unique possibility for gas sensors of satisfying resolution power and sensitivity. Since only one theoretical plate (one absorption and desorption process) is available when using gas sensors, the chiral discrimination is expected to be much more difficult compared to that in GC, where discrimination results from an accumulation of some thousands of absorption−desorption processes. Consequently, in sensorics an approach has to be chosen which leads to clear and significant results, i.e., large discrimination factors or at least the possibility to perform a cross check.

In this context, it seems to be attractive to use neural networks, especially in analogy to the data treatment in natural olfactory systems. However, applying sophisticated pattern recognition tools is only of limited use if, like in our case, the sensor signals and the analyte concentrations show a linear correlation (in the low analyte concentration range, Henry's law holds, see ref 9). So we restricted ourselves to the application of multilinear regression methods (principal component regression, (PCR), principal component analysis (PCA), multilinear regression (MLR)), which already led to excellent results.

In the case of metal coordination and intramolecular entrapment, there exists in most cases only one type of chiral stationary

[†] Center of Interface Analysis and Sensors, Institute of Physical and Theoretical Chemistry.

[‡] Institute of Organic Chemistry.

(1) Franks, N. P.; Lieb, W. R. *Science* **1991**, *254*, 427−430; *Nature* **1994**, *367*, 607−613.

(2) Blaschke, G.; Kraft, H. P.; Fickentscher, K.; Köhler, F. *Drug Res./Arzneim. Forsch.* **1979**, *29*, 1640−1642.

(3) Ide, J.; Nakamoto, T.; Moriizumi, T. *Sens. Actuators A* **1995**, *49*, 73−78.

(4) Schurig, V. In *Chromatographic separations based on molecular recognition*; Jinno, K., Ed.; Wiley: New York, 1996; Chapter 7, pp 371−418.

(5) Meinwald, J.; Thompson, W. R.; Pearson, D. L.; König, W. A.; Rung. T.; Francke, W. *Science* **1991**, *251*, 560−561.

(6) Snopek, J.; Smolkova-Keulemansova, E.; Cserhati, T.; Gahm, K.; Stalcup, A. In *Comprehensive supramolecular chemistry*; Szejtli, T., Osa, T., Eds.; Pergamon: New York, 1996; Vol. 3, Chapter 18, pp 515−571.

(7) Koppenhoefer, B.; Bayer, E. *Chromatographia* **1984**, *19*, 123−130.

(8) Schreier, P.; Bernreuther, A.; Huffer, M. *Analysis of chiral organic molecules, methodology and applications*; Walter de Gruyter: Berlin, 1995; Chapter 3.5.2.1, pp 151−175.

(9) Bodenhöfer, K.; Hierlemann, A.; Noetzel, G.; Weimar, U.; Göpel, W. *Anal. Chem.* **1996**, *68*, 2210−2218.

S0003-2700(96)01299-1 CCC: $14.00

phase material. In the case of amide stationary phases chosen here, however, both enantiomeric forms of the sensitive coating were synthesized and available.

Ide et al.[3] report on discriminating enantiomers of rose oxide and citronellal by using 10-MHz thickness shear mode resonators (TSMRs) with cyclodextrin derivatives as sensing layers. Since they did not specify exactly the enantiomers in the case of rose oxide (two asymmetric C atoms, diastereomers), and, on the other hand, they achieved enantiomeric discrimination even in applying nonchiral stationary phases (ref 3, Table 2) such as squalane or poly(dimethylsiloxane) (PDMS, OV 101), the results are questioned.

To achieve unambiguous results, we thus applied two different transducer principles for discriminating the enantiomers. We chose chiral amides covalently attached to polysiloxane chains (proven to be extremely long-term stable[10]) as sensitive coatings. Both enantiomers of the recognition structure were available, allowing us to perform a cross check of the results and rendering the system more stable with regard to incidential errors. To achieve statistical evidence and to exclude possible artifacts resulting from subtle differences in the vaporization of the analyte enantiomers, the sensor arrays included two nonchiral sensors coated with PDMS (SE-30), five sensors coated with (*R*)-amide, and five sensors coated with (*S*)-amide (for details, see Experimental Section and Figure 1) for each transduction principle.

Mass-sensitive transducers are commonly used for monitoring gases and, in particular, for monitoring volatile organic compounds (VOCs) by using polymer layers as sensitive coatings. The setup consisted of discrete TSMRs operating at a fundamental frequency of 30 MHz. As shown by Sauerbrey,[11] the vibrating frequency of a quartz crystal changes to a first approximation proportionally to the mass deposited onto or removed from the surface:

$$\Delta f = -C f_0^2 \Delta m / A \qquad (1)$$

where Δf is the frequency shift due to the added mass in hertz, C a constant, f_0 the fundamental frequency of the quartz crystal in hertz, and $\Delta m/A$ the surface mass loading in grams per square centimeter. Since the applied analyte concentrations and the TSMR fundamental frequency are rather low (30 MHz), viscosity effects are assumed to contribute only to a small extent to the frequency change due to gas sorption.[12] In any case, the TSMR signal was linear proportional to the analyte content in the gas phase. Changes in conductivity do not affect the device response since the electrodes are located on opposite sides of the quartz disk. In addition, such effects should not affect the chiral discrimination, since they should be identical at comparable analyte concentrations of (*R*)- and (*S*)-enantiomer. For details about resonant mass-sensitive devices, see refs 13 and 14.

In addition to the mass-sensitive device, we employed an array of optical transducers to enhance the reliability of our results by using two independent methods. The fundamentals of reflectometric interference spectroscopy (RIFS) are founded on interference effects occurring at thin transparent films.[15,16] Upon passing a transparent thin polymer film, a light beam is reflected in part at each of the interfaces (air/polymer and polymer/support). As the two reflected beams travel different optical paths, a phase difference is introduced. If the film thickness is small (up to a few micrometers), the difference in optical paths is minute, and even for short coherent (white) light sources interference effects can be observed. These lead to a modulation of reflected light intensity due to constructive and destructive interference. In the case of perpendicular incidence of light, the reflectance R of a thin transparent layer as a function of the wavelength is given by[15]

$$R = R_1 + R_2 + 2(R_1 R_2)^{1/2} \cos(4\pi n d/\lambda) \qquad (2)$$

R_1 and R_2 here denote the Fresnel reflectances of the film interfaces, n the refractive index of the film, d the physical thickness of the film, and λ the wavelength of the incident light. If dispersion effects are neglected, the spectral reflectance pattern can be described by a cosine function using wavenumber units. By absorbing analyte molecules in the thin polymer film, the thickness of the film is slightly changed, causing a shift in the interference spectrum. Consequently, changes in polymer film thickness upon analyte sorption can be determined from the interference spectra with high resolution. Details of this optic method are given in refs 15 and 17.

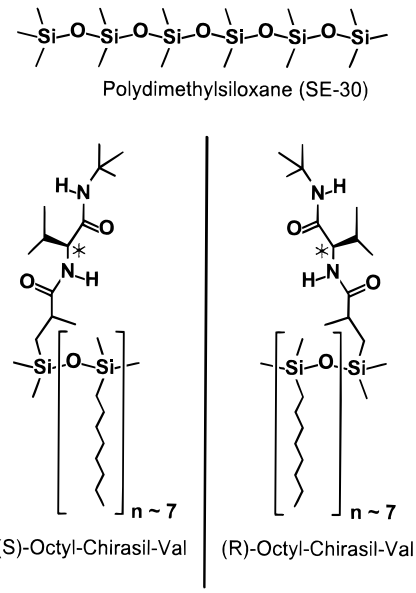

Figure 1. Polymers used for chiral discrimination: nonchiral poly(dimethylsiloxane) (SE-30) and enantioselective (*R*)- and (*S*)-octyl-Chirasil-Val.

EXPERIMENTAL SECTION

Thickness Shear Mode Resonators. The TSMR array consisted of discrete piezoelectric quartz crystals (AT-cut) with gold electrodes operating at a fundamental frequency of 30 MHz (quartz plate thickness, 55.6 μm) purchased from Kristallverarbeitung Neckarbischofsheim (Neckarbischofsheim, Germany).

(10) Hierlemann, A.; Weimar, U.; Kraus, G.; Göpel, W. *Sens. Actuators B* **1995**, *26*, 126−134.
(11) Sauerbrey, G. *Z. Phys.* **1959**, *155*, 206−222.
(12) Martin, S. J.; Frye, G. C.; Senturia, S. D. *Anal. Chem.* **1994**, *66*, 2201−2219.
(13) Grate, J. W.; Martin, S. J.; White, R. M. *Anal. Chem.* **1993**, *65*, 940A−948A; 987A−996A.
(14) Nieuwenhuizen, M. S.; Venema, A. *Sens. Mater.* **1989**, 5, 261−300.
(15) Gauglitz G.; Brecht A.; Kraus G.; Nahm W. *Sens. Actuators B* **1993**, *11*, 21−27.
(16) Brecht A.; Gauglitz G. Fresenius J. *Anal. Chem.* **1994**, *349*, 360−366.
(17) Piehler, J.; Brecht, A.; Gauglitz, G. *Anal. Chem.* **1996**, *68*, 139−143.

Each crystal was powered by an oscillator circuit (bipolar, parallel resonance) constructed in our laboratory. Only one coaxial cable is required for voltage supply and signal transmission. A self-developed scanner operating at frequencies between 100 kHz and 100 MHz was controlled by a PCL 726 interface card (Labtech, Wilmington, MA) in an IBM-compatible PC-AT and allowed for the sequential monitoring of each TSMR output using a Hewlett-Packard 5334B frequency counter. The computer acquired the frequency values via an IEEE 488 interface bus. The first monitored frequency value of each device was set equal to zero; hence, the frequency differences were monitored with reference to this first value.

The frequency outputs of the TSMRs were recorded every 30 s at 0.1-Hz resolution. The gate time of the counter (HP 5334 B) was set to 1 s for all the devices. The sensor responses were given by the frequency difference between gas exposure and purging.

Reflectometric Interference Spectroscopy. All measurements were performed with an array including 12 single sensors, similar to that already described in ref 17. The setup consisted of an infrared-filtered tungsten light source (100 W, stabilized, Osram, Germany) and a diode array spectrometer (MCS 521, 512 diodes, 360−780 nm, Zeiss, Jena, Germany), connected by a fiber-optic coupler bundle (1 mm PMMA, MicroParts, Dortmund, Germany). A single glass rod stuck into the light source and then branched into 13 fibers ensured homogeneity of the light distribution over the fibers. The bundle consisted of 13 Y-shaped optical fibers, each with one 1:2 coupler. One short end of each fiber led to the light source and the other to the diode array via the multiplexer. The single end was connected to the sensing unit. Twelve fibers transferred light to the sensors, an additional one to an uncoated reference substrate. In the present configuration, light from the source was transmitted to a glass substrate coated with the polymer film. After reflection by the optical layer system, the light traveled back via the coupler to the optical multiplexer (Laser Components GmbH, Olching, Germany) and the spectrometer.

One scan of all sensors of the array took 15 s. The glass substrates (refractive index, 1.81; size, 1 cm^2; SFL6, Berliner Glas KG, Berlin, Germany) were mounted into small brass chambers and connected by gas tubings of 6-mm diameter.

Data recording and evaluation was done with homemade software running under Microsoft Windows 95. During each scanning cycle, the thickness of the respective polymer layer was calculated from the interference pattern by evaluating prominent points in the spectrum, as described in ref 18. The changes in optical layer thickness were determined by selecting 10 values of the baseline and 10 of the corresponding sensor signal.

Sensor Coatings. The adsorptive films applied to the transducers consisted of amide-based stationary phase materials for chiral detection in gas chromatography.[7,19] The chosen chiral polymer octyl-Chirasil-Val[19] is a derivative of Chirasil-Val,[7] substituting octylmethylsiloxy groups for dimethylsiloxy groups (Figure 1). The long lipophilic side chains reduce the mutual interaction between the modified valine groups. Both enantiomers of valine were attached to the polysiloxane chains thus providing the two chiral coatings.[19] For the purpose of comparison, both mirror image polymers were synthesized from the same polysiloxane batch to obtain identical contents of the chiral side chains for both optical antipodes. This has been established by ^{1}H-NMR experiments. The thus determined ratio of octylmethylsiloxy groups and methylsiloxy groups with attached valine was 7.1 ± 0.2 for (*R*)- and 7.2 ± 0.3 for (*S*)-octyl-Chirasil-Val. Within experimental error, these values are identical.

Besides the two mirror image polymers, the sensor array included the nonchiral poly(dimethylsiloxane) (SE-30, Macherey & Nagel, Düren, Germany; Figure 1) to check the reproducibility of the gas flow and to additionally monitor the exact analyte concentration. Polysiloxanes and derivatives exhibit low static glass transition temperatures around 150 K and, again, were found to be extremely long-term stable, as reported earlier.[10]

Appropriate coating procedures were chosen for preparing the sensitive layers on the two fundamentally different transducers.

For coating TSMRs, the polymers were dissolved in dichloromethane (concentrations ∼1 mg/mL). The solutions were sprayed onto the cleaned devices with an airbrush using pure nitrogen as a carrier gas. On-line monitoring of the frequency decrease allowed us to determine the frequency shifts due to coating and to calculate the layer thickness assuming a uniform and homogeneous distribution of the polymer over the sensitive surface. The obtained frequency shifts due to coating were around 50 kHz (d = 250 nm) for poly(dimethylsiloxane) and about 60−70 kHz (d = 300−340 nm) for the chiral polymers.

The glass substrates for the RIFS measurements were cleaned in a mixture of H_2SO_4/H_2O_2 (3:2) during 15 min in an ultrasonic cleaner and then rinsed with demineralized water. After this treatment, the polymers were spin-cast on the glass plates from a polymer solution under solvent atmosphere. The applied polymer solutions contained 10% (w/w) of the respective polymer in toluene. The layer thickness was in the range 400−600 nm.

Gas Mixing. The test vapors were generated from specially developed thermocontrolled (T = 283−298 K) vaporizers (details will be described in a forthcoming paper) using synthetic air as carrier gas and then diluted to known concentrations by the computer-driven mass flow controllers. The internal volume of these vaporizers was dramatically reduced, and hence very small quantities of the expensive chiral analytes (minimum 50 μL) could be released at constant concentration. The vapor phase concentrations at the respective temperatures were calculated following the Antoine equation,[20] except for the amino acid derivative (see below). All vapors were mixed and temperature stabilized before entering the thermoregulated chamber. The sensors (all types of coatings were measured simultaneously) were mounted inside a flow-through brass cell, and the measurements were performed at a constant temperature of 303 K. The thermostat used was a microprocessor-controlled Julabo FP 30 MH (Julabo, Seelbach, Germany; precision of 0.01 K guaranteed). The gas flow rate to the sensors was 200 mL/min at a total pressure of 10^5 Pa. The response time of the sensors is in the order of seconds (<1 s). However, the time necessary to reach an equilibrium state in our setup is about 5 min (t_{90} = 120 s) and results from adjusting a constant gas concentration in the chamber (volume, 20 mL) at the chosen flow rate. Typical experiments consisted of alternating

(18) Kraus, G.; Gauglitz, G. *Fresenius' J. Anal. Chem.* **1992**, *344*, 153−157.
(19) Koppenhoefer, B.; Mühleck, U.; Lohmiller, K. *Chromatographia* **1995**, *40*, 718−723.
(20) Riddick, J.; Bunger, A. Organic Solvents. In *Techniques of Chemistry*; Weissberger, A., Ed.; Wiley Interscience: New York, 1970; Vol. II.

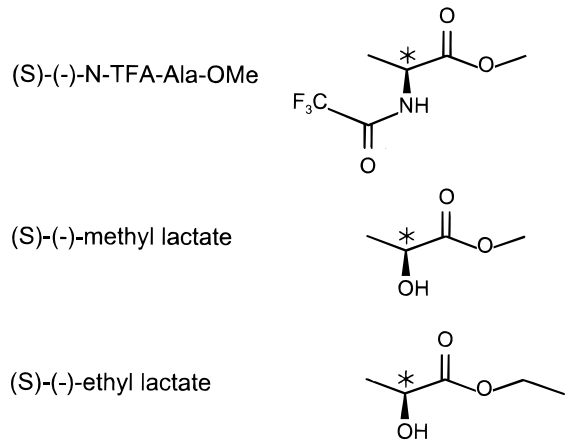

Figure 2. Chiral analytes under investigation in this study: *N*-trifluoroacetylalanine methyl ester (*N*-TFA-Ala-OMe), methyl lactate, and ethyl lactate. Only the respective (*S*)-enantiomers are shown.

exposures to air and vapor. Exposure times of 15 min were followed by 15-min purging of the chamber with synthetic air.

Analytes. The first analyte chosen was *N*-trifluoroacteyl-alanine methyl ester (*N*-TFA-Ala-OMe,[21] Figure 2). *N*-TFA-Ala-OMe is a colorless viscous liquid, and the pure enantiomers as well as the racemate were synthesized ($d_{20} = 1.33$; $n^{20}_D = 1.3967$; *S*, $[\alpha]^{20}_D = -51.34°$; *R*, $[\alpha]^{20}_D = +51.26°$) at the Institute of Organic Chemistry, University of Tübingen. The purity was checked by GC and ^{1}H-NMR experiments. Since the data for applying the Antoine equation were not available, we always give p/p_0 values at the respective temperatures.

Additional analytes (Figure 2) were both enantiomers of methyl lactate (methyl 2-hydroxypropionate, purum; >98%; bp 417−418 K; vapor pressure 155 Pa/283 K; Aldrich-Chemie, Steinheim, Germany), (*S*)-(−)-ethyl lactate (ethyl 2-hydroxypropionate, purum; ∼ 99% (GC); bp 423−426 K; vapor pressure 195 Pa/293 K; Fluka Chemie AG, Buchs, Switzerland), and (*R*)-(+)-ethyl lactate (ethyl 2-hydroxypropionate, puriss.; >99% (GC); bp 423−425 K; vapor pressure 195 Pa/293 K; Fluka Chemie AG).

The respective racemates used in the chiral discrimination section were synthesized (*N*-TFA-Ala-OMe) or purchased (lactates) from the same companies, whereas in the case of determining enantiomeric composition, the racemates were generated in the gas mixing setup by equal analyte gas flows of both enantiomers.

RESULTS AND DISCUSSION

Chiral Discrimination. Our first aim was to demonstrate the ability of our arrays to clearly discriminate optical isomers. In contrast to the already published results[3] on cyclodextrin derivatives, the here-chosen amide polymers offer the unique advantage to perform cross checks, i.e., to sorb each enantiomer of the chiral analyte respectively into each enantiomer of the chiral polymer. On switching from one enantiomer of the analyte to the other, one should observe a crosswise inversion of the sorption behavior of the two enantiomers of the polymer.

In GC experiments, the highest enantiomer discrimination factors using Chirasil-Val derivatives as stationary phase materials have been achieved on injecting amino acids with protected

(21) Trettin, U. Ph.D. Thesis, University of Tübingen, Germany, 1993.

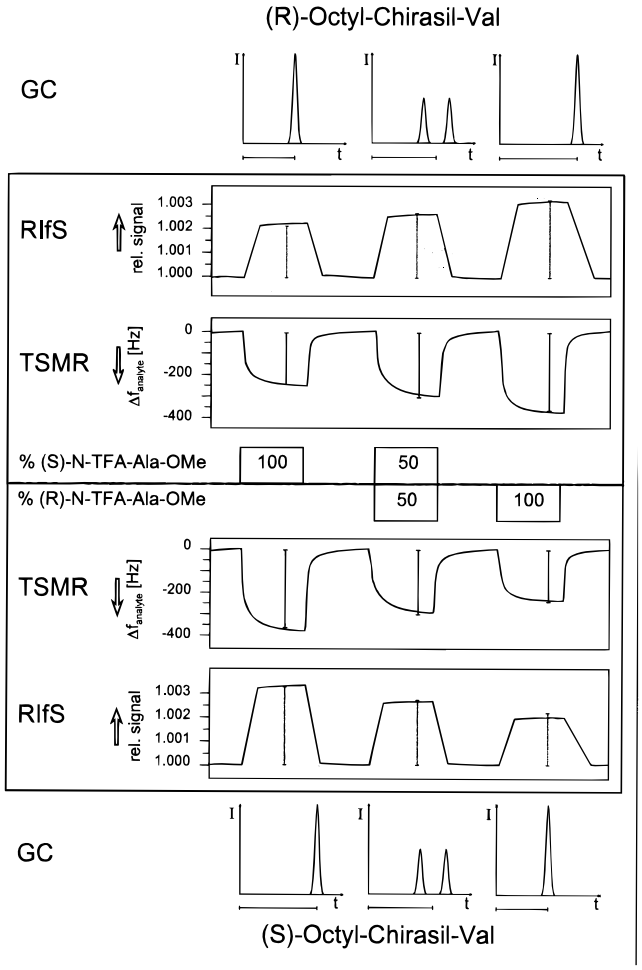

Figure 3. GC results, raw TSMR signals, and normalized (with regard to layer thickness) RIFS responses to (*R*)-, (*S*)-, and racemic *N*-trifluoroacetylalanine methyl ester. The responses of the (*R*)-coatings are displayed in the upper part, those of the (*S*)-polymer in the lower part.

functional groups (the discrimination factors measured in GC experiments are given in Tables 1 and 2). With regard to boiling point and vapor pressure, a very promising candidate was *N*-TFA-Ala-OMe (Figure 2), where the acid group is protected by esterification and the amino group by a trifluoroacetyl group (blocking the amino group is essential for achieving a sufficient vapor pressure and, on the other hand, providing reversibility of the interaction between analyte molecules and the sorption matrix). In a GC column coated with (*R*)-octyl-Chirasil-Val, (*S*)-*N*-TFA-Ala-OMe is eluted in front of the (*R*)-enantiomer (Figure 3). For the mirror image stationary phase, the reverse holds. Consequently, the interactions between (*S*)-analyte and (*S*)-polymer as well as (*R*)-analyte and (*R*)-polymer are stronger than those between the respective (*R*)-/(*S*)-pairs. Corresponding results have been achieved by our sensors. In Figure 3, the raw TSMR signals and the relative changes in optical thickness (RIFS) normalized to the coating thickness are given with respect to the analyte gas composition ((*R*)-, (*S*)-, and racemic analyte). The upper part represents sensor responses and GC results arrived at by using the (*R*)- and the lower part by using the (*S*)-polymer. As can be seen, the analyte uptake (RIFS, TSMRs) of the (*S*)-sensors (represented by relative layer thickness change or frequency shifts) upon exposure to (*S*)-*N*-TFA-Ala-OMe is significantly larger than that of the (*R*)-sensors. For the (*R*)-analyte,

Table 1. α Values Obtained from the Different TSMRs[a]

	coating										
	SE-30	(*R*)-octyl-Chirasil-Val					(*S*)-octyl-Chirasil-Val				
sensor index	E1	R1	R2	R3	R4	R5	S1	S2	S3	S4	S5
$\Delta f_{polymer}$ (kHz)	46.5	59.0	58.5	59.2	69.8	66.7	57.3	57.9	57.7	65.6	69.7
N-TFA-Ala-OMe: $\Delta f_{analyte}/\Delta f_{polymer}[10^{-3}]$, $p/p_{0,298K} = 0.12$ (α from GC, 1.571 ± 0.025 at 303 K)											
(*S*)-enantiomer	0.92	2.12	2.08	2.23	2.16	1.92	3.10	3.06	3.05	2.98	2.98
racemate	0.91	2.46	2.46	2.62	2.55	2.40	2.44	2.42	2.48	2.45	2.46
(*R*)-enantiomer	0.89	2.95	2.94	3.09	2.97	2.81	1.92	1.89	1.94	1.92	1.93
discrimination factor α	1.034	0.718	0.709	0.721	0.728	0.682	1.617	1.622	1.574	1.553	1.543
mean discrimination factor				0.712					1.582		
SD α				0.018					0.036		
$\alpha' = \alpha^{-1}$		1.392	1.410	1.387	1.373	1.466					
mean discrimination factor				1.411							
SD α′				0.036							
Methyl Lactate: $\Delta f_{analyte}/\Delta f_{polymer}[10^{-3}]$, 390 ppm (α from GC, 1.130 ± 0.002 at 303 K)											
(*S*)-enantiomer	1.45	3.04	3.36	3.38	3.13	2.96	2.84	2.84	2.99	3.23	3.33
racemate	1.42	2.85	3.14	3.17	2.95	2.79	2.98	2.99	3.13	3.39	3.48
(*R*)-enantiomer	1.46	2.71	2.98	3.01	2.81	2.66	3.18	3.20	3.34	3.61	3.70
discrimination factor α	0.991	1.120	1.124	1.124	1.116	1.112	0.895	0.887	0.895	0.895	0.901
mean discrimination factor				1.119					0.895		
SD α				0.005					0.005		
$\alpha' = \alpha^{-1}$							1.117	1.127	1.117	1.117	1.110
mean discrimination factor									1.118		
SD α′									0.006		
Ethyl Lactate: $\Delta f_{analyte}/\Delta f_{polymer}[10^{-3}]$, 390 ppm (α from GC, 1.118 ± 0.003 at 303 K)											
(*S*)-enantiomer	3.24	8.00	8.11	8.72	7.93	7.69	6.87	6.59	7.07	6.75	6.89
racemate	3.32	7.76	7.83	8.51	7.70	7.37	7.26	7.21	7.36	7.30	7.43
(*R*)-enantiomer	3.26	7.11	7.22	7.79	7.10	6.86	7.61	7.42	7.85	7.51	7.68
discrimination factor α	0.996	1.125	1.123	1.120	1.118	1.121	0.902	0.889	0.901	0.899	0.897
mean discrimination factor				1.121					0.898		
SD α				0.003					0.005		
$\alpha' = \alpha^{-1}$							1.108	1.125	1.110	1.112	1.115
mean discrimination factor									1.114		
SD α′									0.006		

[a] Coatings, frequency shifts due to coating, and sensor indexes are given in the headings. The sensor signals normalized to the coating thickness for (*S*)-enantiomer, (*R*)-enantiomer, and racemate as well as sensor α (α′) values and mean values with standard deviations (SD) are listed for each analyte. The respective GC α values are given in the analyte headings.

the above mentioned crosswise inversion is experimentally proven: stronger sorption into the (*R*)-polymer. As expected, the signals of the chiral sensors upon exposure to the racemic mixture (racemate) match. With regard to the plots of the enantiomeric analytes, these racemate signals are of intermediate heights. In the case of the racemates, the sensor signal intensities are correlated to the retention time of the focal point of the two separate enantiomer peaks of identical area.

In the case of *N*-TFA-Ala-OMe, the differences in the sensor response plots ((*R*)-, (*S*)-, and racemate) are sufficiently large with regard to noise and variation of the sensor signals.

Working on the results of the lactates (minor variation in the sensor signals upon exposure to different enantiomers), we decided to analyze the responses to the chiral analytes separately for each sensor and to evaluate the ratios of (*S*)- to (*R*)-signals or the inverse. In GC, a discrimination factor α (α always larger than zero) is defined as ratio of the net retention times:[22]

$$\alpha_{GC} = \frac{t_{(S)-\text{analyte}} - t_0}{t_{(R)-\text{analyte}} - t_0} \qquad \text{for } t_{(S)-\text{analyte}} > t_{(R)-\text{analyte}} \quad (3)$$

t denotes the time when the analyte peak appears, t_0 the dead time of the column. In analogy, we propose to define a chiral discrimination factor for sensors:

$$\alpha_{sens} = \frac{\Delta f_{(S)-\text{analyte}}}{\Delta f_{(R)-\text{analyte}}} \quad \text{or} \quad \alpha_{sens} = \frac{\Delta nd_{(S)-\text{analyte}}}{\Delta nd_{(R)-\text{analyte}}} \quad \text{and}$$

$$\alpha'_{sens} = \frac{\Delta f_{(R)-\text{analyte}}}{\Delta f_{(S)-\text{analyte}}} \quad \text{or} \quad \alpha'_{sens} = \frac{\Delta nd_{(R)-\text{analyte}}}{\Delta nd_{(S)-\text{analyte}}} \quad (4)$$

Here, Δf denotes the frequency shift and Δnd the change in optical thickness (n, refraction index; d, layer thickness) of the sensors exposed to the same concentration of respective enantiomer of the analyte. α denotes the ratio of two sorption equilibrium constants, $K_{(R)-\text{analyte}}$ and $K_{(S)-\text{analyte}}$, and does not vary with changing layer thickness, since the constants both depend on the layer thickness in the same way. In contrast to the GC theory, where α is always larger than 1, we here choose a rigid definition and thus allow values smaller than 1 as well. Thus, it is easier to demonstrate the inversion behavior and to describe changing affinities between the analyte enantiomers and the chiral coatings.

In this context, an important aspect concerns the concentration dependence of the discrimination factor. From our experiments, it can be derived as a rule of thumb that the discrimination factor is constant at an occupation ratio below 10% of all enantioselective groups by the analyte molecules. In measuring at low analyte concentrations, we made sure to be below or around this limit.

(22) Weinstein, S.; Feibush, B.; Gil-Av, E. *J. Chromatogr.* **1976**, *126*, 97−111.

Table 2. α Values Obtained from the Different RIFS Transducers[a]

	coating										
	SE-30	(*R*)-octyl-Chirasil-Val					(*S*)-octyl-Chirasil-Val				
sensor index	E1	R1	R2	R3	R4	R5	S1	S2	S3	S4	S5
N-TFA-Ala-OMe: $\Delta nd_{analyte}/nd_{polymer}[10^{-3}]$, $p/p_{0,298K} = 0.12$ (α from GC, 1.571 ± 0.025 at 303 K)											
$nd_{polymer}$ (nm)	618	729	711	679	700	688	721	722	734	732	731
(*S*)-enantiomer	0.83	1.93	1.87	1.45	1.43	2.05	3.13	3.03	3.21	3.14	3.78
racemate	0.83	2.57	2.47	1.71	1.91	2.66	2.59	2.46	2.63	2.54	3.08
(*R*)-enantiomer	0.86	3.22	3.07	2.31	2.39	3.29	2.16	2.14	2.17	2.05	2.50
discrimination factor α	0.96	0.60	0.61	0.62	0.60	0.62	1.45	1.42	1.48	1.53	1.51
mean discrimination factor				0.61					1.48		
SD α				0.011					0.041		
$\alpha' = \alpha^{-1}$		1.67	1.64	1.60	1.67	1.61					
mean discrimination factor				1.64							
SD α′				0.030							
Methyl Lactate: $\Delta nd_{analyte}/nd_{polymer}[10^{-3}]$, 390 ppm (α from GC, 1.130 ± 0.002 at 303 K)											
$nd_{polymer}$ (nm)	586	574	562	581	575	563	577	565	591	596	568
(*S*)-enantiomer	1.13	3.21	2.86	3.08	2.89	3.08	2.89	2.46	3.11	3.34	3.22
racemate	1.13	2.99	2.64	2.83	2.67	2.86	2.98	2.52	3.21	3.45	3.32
(*R*)-enantiomer	1.12	2.78	2.46	2.63	2.49	2.67	3.21	2.64	3.43	3.61	3.45
discrimination factor	0.99	1.16	1.16	1.16	1.16	1.15	0.90	0.93	0.91	0.93	0.93
mean discrimination factor				1.16					0.92		
SD α				0.005					0.013		
$\alpha' = \alpha^{-1}$							1.11	1.07	1.10	1.08	1.07
mean discrimination factor									1.09		
SD α′									0.015		
Ethyl Lactate: $\Delta nd_{analyte}/nd_{polymer}[10^{-3}]$, 390 ppm (α from GC, 1.118 ± 0.003 at 303 K)											
$nd_{polymer}$ (nm)	643	758	710	715	705	705	722	735	768	806	642
(*S*)-enantiomer	4.44	10.73	11.3	9.47	9.29	11.0	10.0	10.67	9.70	9.77	10.37
racemate	4.40	9.93	10.5	8.81	8.73	10.2	10.3	11.0	10.1	10.0	10.67
(*R*)-enantiomer	4.48	9.45	9.99	8.43	9.29	10.7	10.9	11.6	10.9	10.7	11.33
discrimination factor	1.01	1.14	1.14	1.12	1.10	1.13	0.91	0.91	0.89	0.91	0.92
mean discrimination factor				1.13					0.91		
SD α				0.015					0.010		
$\alpha' = \alpha^{-1}$							1.10	1.10	1.12	1.10	1.09
mean discrimination factor									1.10		
SD α′									0.011		

[a] Coatings and sensor indexes are given in the headings. A new set of RIFS sensors was prepared for each analyte, and the corresponding layer thicknesses are noted. The relative sensor signals normalized to the coating thickness for (*S*)-enantiomer, (*R*)-enantiomer, and racemate as well as sensor α (α′) values and mean values with standard deviations (SD) are listed for each analyte. The respective GC α values are given in the analyte headings.

At higher concentrations, the discrimination factor decreases and shows a tendency toward 1, i.e., no more chiral discrimination. By taking into account the molecular weights of *N*-TFA-Ala-OMe (213 g/mol), methyl lactate (104 g/mol), ethyl lactate (118 g/mol), and a chain segment of the polymer including one enantioselective valine group (1480 g/mol, octyl:valine = 7:1 as determined by ^{1}H-NMR), the maximum occupation ratio (OR) of the chiral groups in the matrix can be estimated:

$$\text{occupation ratio (OR)} = (\Delta f_{analyte} M_{polymer})/(\Delta f_{polymer} M_{analyte}) \quad (5)$$

Here, M denotes the molecular mass of the analyte molecule (analyte) or chain segment (polymer), $\Delta f_{analyte}$ the frequency shift due to analyte absorption, and $\Delta f_{polymer}$ the frequency shift due to coating. In this simple model, it is assumed that the analyte molecule exclusively interacts with the enantioselective group. Since $\Delta f_{analyte}$ represents the sum of interactions of the analyte molecules with the backbone and the enantioselective groups, the actual occupation is lower than this maximum value. The frequency shifts due to coating ranged around 60 kHz, and the maximum sensor signals were around 400 Hz for *N*-TFA-Ala-OMe, 200 Hz for methyl lactate, and 600 Hz for ethyl lactate. The deduced maximum occupation ratios hence amounted to 5% for methyl lactate and *N*-TFA-Ala-OMe and 12% for ethyl lactate. In all cases, we observed a constant discrimination factor with respect to varying analyte concentrations.

The chiral discrimination factors of the lactates as determined in GC measurements (given in Tables 1 and 2, measured on a fused-silica capillary column) are considerably lower than that of the amino acid derivative. The lactates hence constitute a more realistic test system for our sensors with regard to performance and resolution. In addition, considerable quantities of lactic esters are industrially produced in enantiomeric purity; hence, a practical application of the sensors could be realized here. Previous GC measurements showed stronger interactions between the mixed pairs (*S*)-lactate/(*R*)-polymer and (*R*)-lactate/(*S*)-polymer. This is consistent with our results: The enrichment in the polymer is larger in the case of (*S*)-/(*R*)- or (*R*)-/(*S*)- pairs than it is for (*S*)-/(*S*)- or (*R*)-/(*R*)- pairs.

In Figure 4, the chiral discrimination factors of five (*R*)-sensors (R1−R5, TSMRs) and five (*S*)-sensors (TSMRs) are displayed. With regard to the (*R*)-sensors, the α factors as defined in GC and sensorics are identical: values larger than 1. They differ in

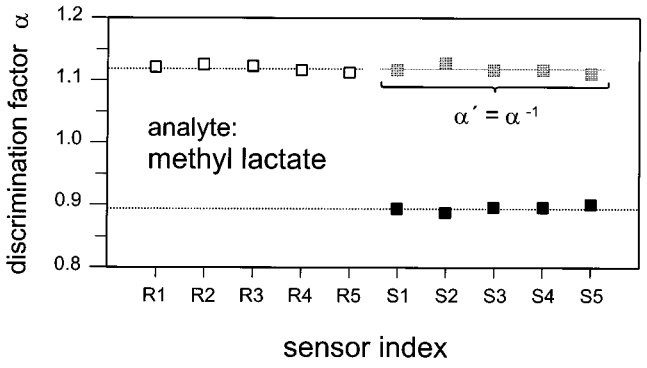

Figure 4. Discrimination factors of methyl lactate obtained by five different (*R*)- and (*S*)-sensors. For the (*S*)-sensors, the α′ values are shown as well to demonstrate the inversion symmetry.

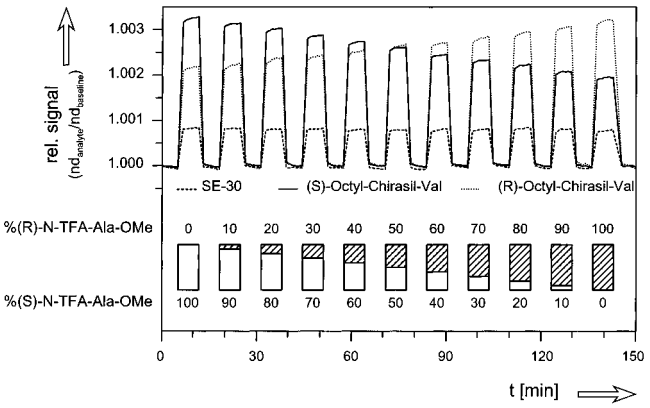

Figure 5. Relative RIFS sensor signals (normalized with regard to the layer thickness without analyte gas; for further details, see text) of two chiral sensors ((*S*)-sensor, solid line; (*R*)-sensor, points) and an additional SE-30 sensor (dashed line) upon exposure to mixtures of different enantiomer contents (in %) of *N*-TFA-Ala-OMe.

the case of the (*S*)-sensors. Here, the α′ values (corresponding to the respective GC α values) are additionally shown to demonstrate the symmetry of the analyte/polymer system with regard to inversion (perfect matching of the (*R*)- α and (*S*)- α′ values). On the other hand, this figure helps to elucidate the reasons behind our definition: at first glance, it can be seen which enantiomer is absorbed to a larger extent into the respective chiral polymer.

Table 1 comprises the data (α, α′ values) obtained with TSMRs (and GC values); Table 2 the RIFS results (and GC values) for the three analytes. All average α values obtained from a subset of (*R*)- or (*S*)-sensors match within experimental error the respective GC values given in the analyte headline. Whereas the normalized (with respect to the coating thickness) sensor signals show considerable fluctuations, the variation of the α values from sensor to sensor is very low since all sensor-specific factors (layer thickness, morphology, etc.) cancel out. This is of special interest in the case of the RIFS measurements, since the light spot (fiber diameter, 1 mm) is very small (0.76 mm^2) compared to the electrode surface of the TSMRs (14 mm^2, both sides coated). Hence, the information results from a small quantity of sensing material and, therefore, is more subject to specific local variations, whereas in the case of the TSMRs the mass uptake is averaged over a large area.

The evaluation of the α values is in complete agreement with GC methods, where always the retention times of different analytes on the same stationary phase are analyzed. Comparing the results of different columns with the same stationary phase material would lead to significant variations as well.

The values of the nonchiral SE-30 sensors are subject to only small statistical fluctuations; the respective analyte flow, hence, is excellently reproducible. In the case of *N*-TFA-Ala-OMe, the slightly varying SE-30 α values (1.034, 0.96) indicate that the analytes may contain minimal contaminations, since this value should be exactly 1 (compare the lactates). The lack of perfect symmetry (α, α′) is an additional hint.

Significant differences exist between the signals of the chiral sensors upon exposure to the analyte enantiomers. In the case of the amino acid derivative (p/p_0 values), the largest α values could be achieved; the standard deviations (SD), however, are larger as well. In the case of the lactates, the discrimination factors are considerably lower but highly reproducible with a low standard deviation. For both esters, methyl lactate and ethyl lactate, the distinction of the enantiomers can be explicitly shown. The statistical fluctuations and errors are low and hence do not affect the chiral discrimination of the analytes under investigation here.

Enantiomeric Purity/Composition. After having successfully discriminated the optical antipodes of the different analytes, we tried in a second step to determine the enantiomeric composition, thus testing the resolution power of our system. For this purpose, the sensor arrays were exposed to mixtures of different contents of the respective analyte enantiomers. These mixtures were prepared by joining the two separate gas flows of the enantiomers according to the adjusted values. We always recorded a calibration set consisting of five identical runs each including 11 different ratios of the enantiomers (100/0, 90/10, 80/20, ..., 0/100; compare Figure 8), and, in addition, an independent test data set containing only a few of the data points already used for calibration (compare Figure 9). The mathematical tools used to evaluate the data only comprised simple multilinear regression (MLR, performed with Excel from Microsoft), principal component analysis (PCA), and principal component regression (PCR) using Unscrambler provided by CAMO[23] (Trondheim, Norway).

Sometimes it is possible to determine the enantiomeric composition from the raw sensor signals without applying any mathematical tool. In the case of the amino acid derivative, the discrimination factors are comparatively high; hence, trends can be extracted, e.g., from the RIFS sensor signals of Figure 5. The relative sensor signals (change in optical thickness due to gas exposure related to the layer thickness without analyte gas) are displayed, and it can be seen that the maximum change in optical thickness was in the range of 0.003 of the respective polymer layer thickness. The sensor response of the SE-30 sensor was identical for the 11 sequential exposures. This indicated the precision of the adjusted gas flows and, on the other hand, served as a reference for the chiral sensors exposed to the same gas atmosphere. These chiral sensors (selected with respect to equal layer thickness) showed systematic variations (signal increase or decrease) with changing enantiomer composition of the analyte. Every 10% step in changing composition is easy to recognize. The

(23) *Unscrambler, Software and Documentation for Multivariate Data Analysis with PCA, PCR and PLS*; CAMO A/S: Trondheim, Norway, 1996; Version 6.0.

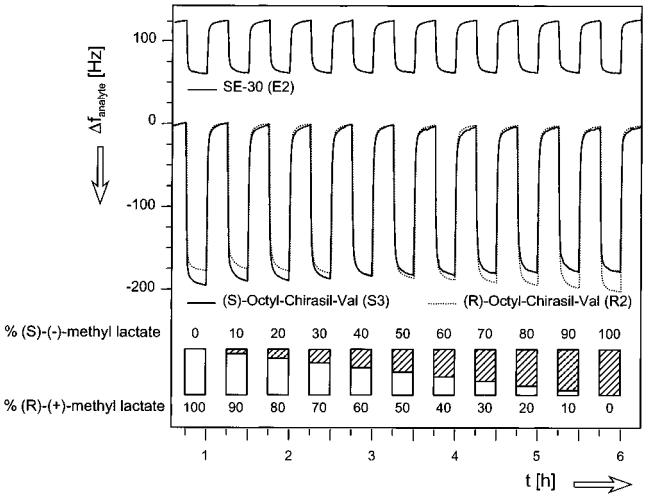

Figure 6. Raw TSMR signals (frequency shifts in hertz) of two chiral sensors ((*S*)-sensor, solid line; (*R*)-sensor, points) of similar layer thickness and an additional SE-30 sensor (solid line) upon exposure to mixtures of different enantiomer contents (in %) of methyl lactate.

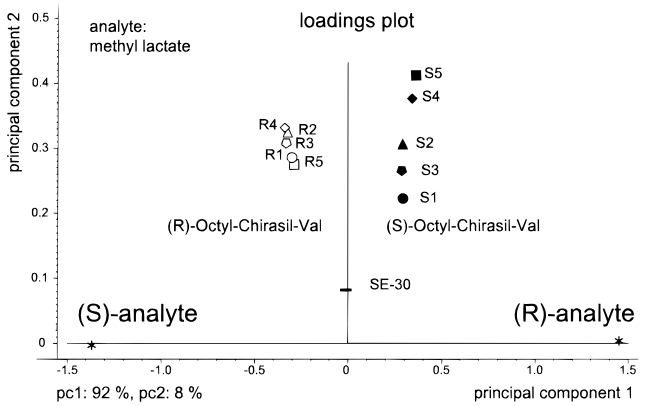

Figure 7. Loadings plot of a PCA analysis of signals obtained from the TSMR array. Open symbols represent the (*R*)-sensors, black symbols the (*S*)-sensors, and a black rectangle the SE-30 sensor. The points of (*R*)- and (*S*)-enantiomer of methyl lactate are visualized by stars.

signal of the (*S*)-sensor increased with increasing (*S*)-analyte concentration, and vice versa for the (*R*)-sensor. This is consistent with the results discussed above in the Chiral Discrimination section.

In Figure 6, a corresponding TSMR response plot is shown for methyl lactate. Although the discrimination factor is much smaller (∼1.1), trends could be identified even here. Again, the SE-30 sensor proved the additivity of the enantiomer gas flows. The (*S*)-sensor in this case, however, showed decreasing signals with increasing (*S*)-analyte content of the mixture, owing to the lower affinity between (*S*)-sensor/(*S*)-analyte if compared to (*R*)-sensor/(*S*)-analyte (see discussion above). The signals of both chiral sensors again nearly matched for the racemic mixture.

In a thorough and enhanced analysis, the data of the three analyte enantiomer mixtures were comparatively processed by MLR methods, PCR, and PCA. First, the PCA (qualitative analysis) results (from TSMR measurements) are presented. The loadings plots for methyl lactate (Figure 7) show the old coordinates (sensors) and the pointers of the analytes in the vector space of the first two principal components (new coordinates). The first principal component contains 92% of the relevant information; the second principal component contains only 8% and most of the experimental noise. Consequently, the analysis problem can be solved to a large extent in a one-dimensional vector space. In other words, the scattering in the first principal component, which is aligned along the largest sensor response gradient, determines the resolution of the PCA analysis. The (*R*)-sensors are located close to the (*S*)-analyte pointer and the (*S*)-sensors close to the (*R*)-analyte pointer, thus indicating the preferential sorption of (*R*)-analyte into (*S*)-polymer and (*S*)-analyte into (*R*)-polymer. An important point is the location of the SE-30 vector at the zero value of principal component 1. The SE-30 sensors hence have no effect on the chiral discrimination, which is to be expected, provided that the gas mixing setup and the vaporizers work correctly. The zero position of achiral sensing layers in PCA loadings plots therefore constitutes an important feature in every chiral discrimination.

In Figure 8, the accompanying scores plot is shown. The scores plot represents a projection of the sensor responses of the array in the vector space of the new coordinates (principal components). The 55 calibration points (five subsequent runs at 11 points each) form 11 groups, corresponding to the 11 adjusted enantiomeric compositions (10% steps, compare Figure 8) of the analyte. Each group includes five points from the five subsequent calibration runs. With regard to information content and scattering of the points, the same arguments as discussed in the context of the loadings plot are valid. Hence, the scattering in direction of the first principal component is crucial. The variations in the second principal component are mainly due to noise and statistical fluctuations in the different runs. Even in the case of methyl lactate with a quite small α value (α ≈ 1.1; such small values are characteristic for most practical discrimination problems), the 11 five-point groups (five subsequent runs) are clearly separated from each other. Even at 5% changes in the enantiomeric composition, the groups would not overlap, and the resolution of the array would be sufficient. This simple qualitative evaluation already shows that the determination of enantiomeric purities at 10% resolution is possible with each of the sensor arrays described in this study.

The results obtained in qualitative analysis (PCA) could be verified by applying quantitative methods like MLR and PCR. Figure 9 displays PCR results (TSMRs) again for the example of methyl lactate. The *x*-axis represents the adjusted values, the *y*-axis the corresponding values predicted by PCR for the independent test set, which additionally included mixtures at 5% variations which were not present in the calibration set. For comparison purposes, five (*R*)-sensors, five (*S*)-sensors, and one SE-30 sensor were chosen for the left plot; for the right plot we evaluated only three sensors, one (*R*)-, one (*S*)-, and one SE-30-sensor, and thus minimized the array. The ideal correlation is marked by a straight line intersecting the origin. In both cases, the data points are located very close to this straight line. Hence, the quantitative prediction of the enantiomeric composition of a given compound by means of sensors is confirmed. In Tables 3 and 4, the results achieved with MLR, PCR, and a simple direct evaluation method are collected. For both types of sensors (TSMR and RIFS), several array configurations were tested. The mean absolute errors (*E*(AE) in % enantiomeric composition) for predicting the calibration set and the independent test data set from the raw sensor signals are listed. They are somewhat lower for the TSMRs (better signal−noise ratio) compared to those from the RIFS measurements. The first column contains the results

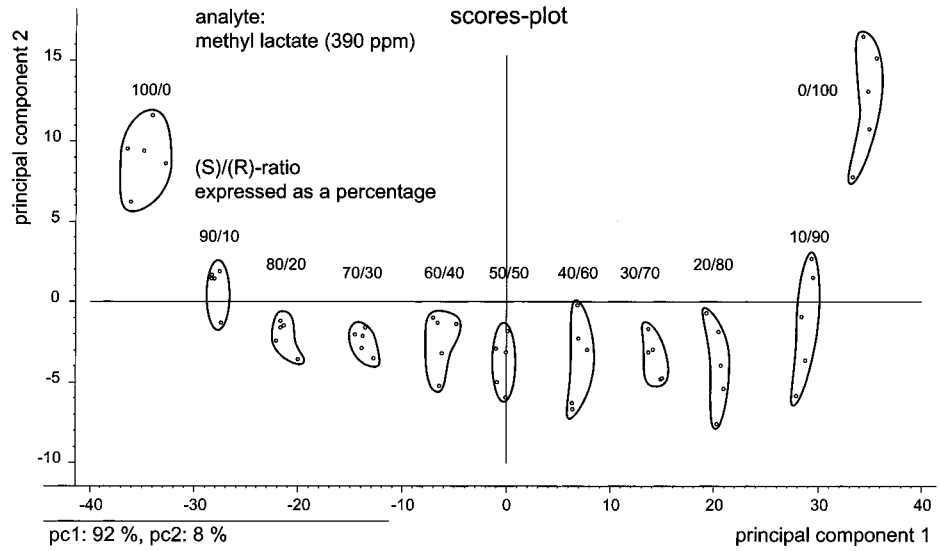

Figure 8. Scores plot of a PCA analysis (TSMR array response) of mixtures of different enantiomeric composition of methyl lactate. The small circles mark the data points of five subsequent runs at 10% variation of the enantiomeric composition. Each five data points of identical composition form clearly distinct groups.

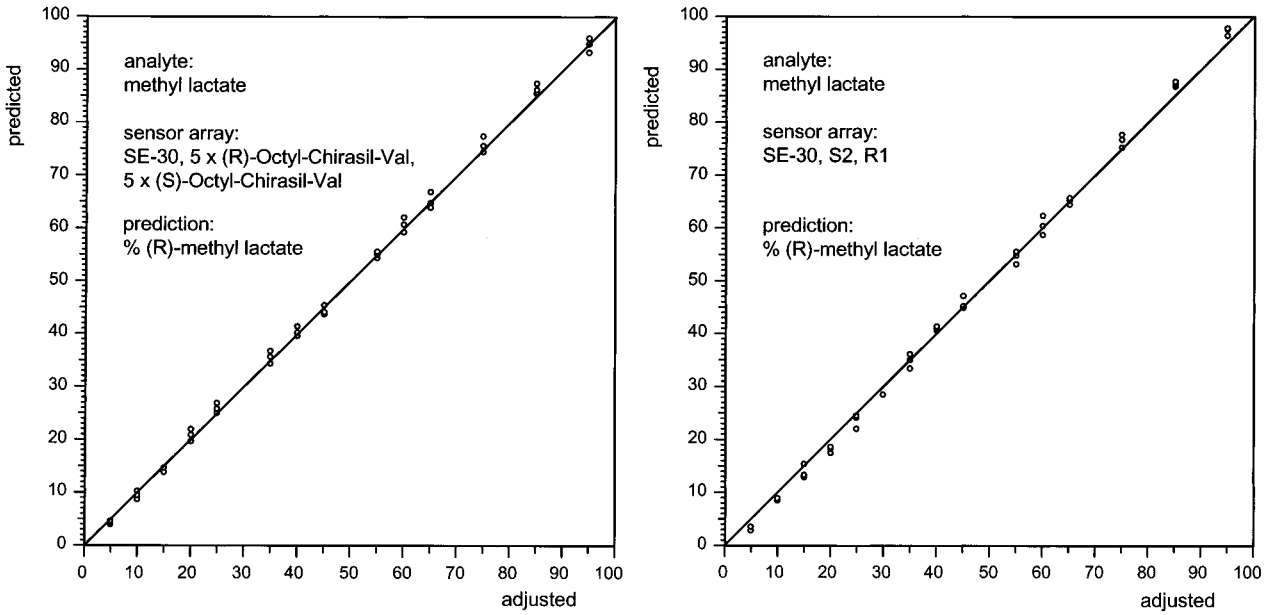

Figure 9. Predicted vs adjusted enantiomeric compositions of methyl lactate. The ideal correlation is marked by a straight line intersecting the origin. The test set comprised 45 points; the array included 11 sensors (left) and three sensors (right).

arrived at by the whole array of 11 sensors; in the second column, SE-30 is left out; in the third the array included one chiral sensor of each type and one nonchiral; in the fourth two mirror image chiral sensors are evaluated; and in the fifth and sixth columns only one type of chiral sensor and SE-30 formed the array. The prediction on the test set was always approximately by a factor of 2 (TSMRs) or 6 (RIFS) worse than that on the calibration set. Nevertheless, the errors of most of the predictions were below 1.5% (TSMRs) or 4−5% (RIFS). Therefore, it is possible to reduce the array to two or three (including SE-30) sensors without a major loss of resolution. In the case of using only one chiral sensor, the errors significantly increased (4−10%), especially in determining the lactates with the comparatively low α values. In the case of *N*-TFA-Ala-OMe, the large α value provided lower errors (TSMR, 0.8−1.2%; RIFS, 2.5−3.5%). The discrimination factor (α) hence constitutes an important criterion in determining the array discrimination and resolution capability. As can be deduced from these results, applying only one type (enantiomer) of chiral sensors distinctly reduces the resolution power of the array, especially in the case of low α values.

The results of the multilinear regression were somewhat better than those of PCR. This indicated that the sensor response model was nearly perfectly linear and the superposition principle holds for the mixtures of both enantiomers (no mixing effects occurring).

We also listed the results of a simple signal evaluation method: The response of an arbitrarily chosen (*R*)-sensor was subtracted from that of an (*S*)-sensor or vice versa. These results were comparable to those of column 3 or 4 of Tables 3 and 4. Hence, for practical applications, this simple evaluation is favorable with regard to the simplicity of the method.

Thermodynamic Data. TSMR measurements of the α values at varying temperatures were performed with the intention to get information about the enthalpy difference between sorbing the

Table 3. Mean Values of the Absolute Errors, *E*(AE), Achieved with MLR, PCR, and a Simple Subtraction Method from TSMR Signals[a]

	n	*R*	*S*	n	*R*	*S*	n	*R*	*S*	n	*R*	*S*	n	*R*	*S*	n	*R*	*S*	n	*R*	*S*
array configuration	1	5	5	–	5	5	1	1	1	–	1	1	1	1	–	1	–	1	–	1	1
Multilinear Regression (MLR)																					
N-TFA-Ala-OMe, *E*(AE)																					
calibration set		0.31			0.31			0.45			0.45			0.87			0.92			0.45[b]	
test set		0.66			0.66			0.65			0.66			1.12			0.98			0.70[b]	
Methyl Lactate, *E*(AE)																					
calibration set		0.44			0.44			0.67			0.67			4.17			4.44			0.73[b]	
test set		0.93			0.94			1.41			1.41			6.20			7.32			1.45[b]	
Ethyl Lactate, *E*(AE)																					
calibration set		0.26			0.26			0.50			0.96			3.46			4.58			0.95[b]	
test set		0.52			0.53			1.00			1.43			9.96			10.48			1.34[b]	
Principal Component Regression (PCR)																					
N-TFA-Ala-OMe, *E*(AE)																					
calibration set		0.57			0.57			0.50			0.50			0.87			0.92				
test set		0.90			0.90			0.88			0.88			1.12			0.97				
Methyl Lactate, *E*(AE)																					
calibration set		0.94			0.94			0.68			0.68			4.17			4.44				
test set		0.87			0.85			1.44			1.44			6.26			7.32				
Ethyl Lactate, *E*(AE)																					
calibration set		0.69			0.69			0.96			0.96			3.46			4.58				
test set		1.48			1.48			1.31			1.30			9.96			10.48				

[a] In the headings the array configurations (number of applied (*R*)-, (*S*)-, and nonchiral (n, SE-30) sensors) are displayed. The mean values for the calibration (55 points) and the separate test data set (45 points) are given in % enantiomeric composition for each analyte. [b] By simple subtraction.

Table 4. Mean Values of the Absolute Errors, *E*(AE), Achieved with MLR, PCR, and a Simple Subtraction Method from RIFS Sensor Signals[a]

	n	*R*	*S*	n	*R*	*S*	n	*R*	*S*	n	*R*	*S*	n	*R*	*S*	n	*R*	*S*	n	*R*	*S*
array configuration	1	5	5	–	5	5	1	1	1	–	1	1	1	1	–	1	–	1	–	1	1
Multilinear Regression																					
N-TFA-Ala-OMe, *E*(AE)																					
calibration set		0.55			0.56			0.81			0.81			3.10			3.49			2.44[b]	
test set		3.38			3.35			3.85			3.35			3.42			2.59			4.61[b]	
Methyl Lactate, *E*(AE)																					
calibration set		0.36			0.42			0.61			0.68			2.88			3.65			1.34[b]	
test set		3.46			2.98			4.77			4.53			7.12			7.74			4.47[b]	
Ethyl Lactate, *E*(AE)																					
calibration set		0.39			0.41			4.22			4.51			5.11			4.92			1.89[b]	
test set		1.64			1.40			4.46			4.83			8.08			7.50			4.73[b]	
Principal Component Regression																					
N-TFA-Ala-OMe, E(AE)																					
calibration set		2.04			2.04			0.83			0.83			2.91			2.59				
test set		3.24			3.38			3.86			3.85			3.64			3.55				
Methyl Lactate, *E*(AE)																					
calibration set		1.61			1.60			0.79			0.80			2.86			3.37				
test set		3.55			3.03			4.77			4.53			7.23			6.93				
Ethyl Lactate, *E*(AE)																					
calibration set		1.13			1.12			4.57			4.57			6.63			5.82				
test set		2.55			1.41			4.68			4.82			8.80			6.12				

[a] In the headings, the array configurations (number of applied (*R*)-, (*S*)-, and nonchiral (n, SE-30) sensors) are displayed. The mean values for the calibration (55 points) and the separate test data set (45 points) are given in % enantiomeric composition for each analyte.

(*S*)-enantiomer and the (*R*)-enantiomer of a certain analyte into the same chiral polymer. Since the sensor signals were proportional to the applied analyte concentrations at any temperature, we assumed mass-loading effects to be dominant.[12] Two (*R*)- and two (*S*)-sensors and additionally two SE-30 sensors were chosen for these measurements. The sensors were subsequently exposed to an identical preset concentration of both methyl lactate enantiomers. The SE-30 sensors acted only as a reference to see whether both enantiomer concentrations are identical. Increasing the temperature by 10 K effects a reduction of the sensor signals by roughly a factor of 2. The α values of methyl lactate were determined from the sensor responses at temperatures between 333 and 283 K. The α value is related to the $\Delta\Delta G^0$ value via the following expression:[7]

$$-\Delta\Delta G^0 = RT \ln \alpha \qquad (6)$$

$\Delta\Delta G^0$ here denotes the enantiomeric difference in free enthalpy for transition of 1 mol of analyte from the gas to the liquid phase in the polymer (polymer sorption). R is the universal gas constant. The average $\Delta\Delta G^0$ values extracted this way (from Tables 1 and 2) (at 303 K) for the different analytes were as follows: *N*-TFA-Ala-OMe, -1050 ± 100 J/mol, ethyl lactate, -275 ± 15 J/mol; methyl lactate, -285 ± 15 J/mol.

Determining the discrimination factor (α) at different temperatures allowed us to calculate the difference in enthalpy ($\Delta\Delta H^0$) and entropy ($\Delta\Delta S^0$) of enantiomer sorption into the polymer, according to[24]

$$\ln \alpha = \frac{-\Delta\Delta H^0}{R}\frac{1}{T} + \frac{\Delta\Delta S^0}{R} \qquad (7)$$

In performing such measurements, another advantage of using sensors is revealed: Dosing the analyte simultaneously to an array of sensors at different temperatures provides generalizability of the achieved values in a shorter time than sequentially measuring with several columns. The reproducibility in such a parallel approach is better as well, since the measuring conditions are identical.

In Figure 10, the plots of ln α vs $1/T$ are displayed for methyl lactate using two (*R*)- and two (*S*)-sensors. The ln α values for the two different enantiomers of the coating are located approximately in mirror symmetry to the abscissa. There is a clear increase in the discrimination factor with decreasing temperature, i.e., the enantiomeric discrimination capability of the array increases. Evaluating the slopes led to $\Delta\Delta H^0$ values of -1.4 ± 0.1 kJ/mol in the case of the (*R*)-sensors and $+1.2 \pm 0.2$ kJ/mol in the case of the (*R*)-sensors. Consequently, the average enthalpy difference in absorbing the two enantiomers of methyl lactate into the present chiral polymer is around 1.3 kJ/mol. The corresponding value obtained by GC measurements was 1.1 kJ/mol.

CONCLUSION

First, it could be unambiguously established that chiral discrimination by gas sensors is possible. The coincidence of the results achieved with two independent transducer principles at two independent gas mixing stations, as well as the successful performed cross checks and observed inversion symmetry, strongly supports this statement. In addition, the matching of the sensor α values with GC α values provides further evidence.

(24) Lohmiller, K.; Bayer, E.; Koppenhoefer, B. *J. Chromatogr.* **1993**, *634*, 65−67.

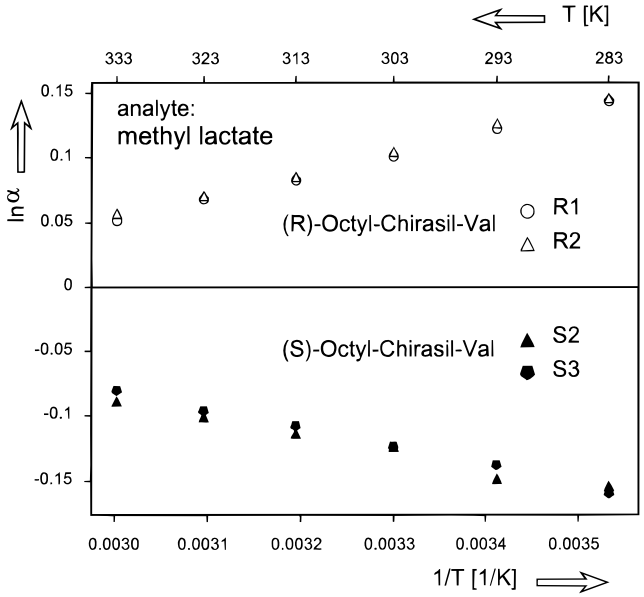

Figure 10. Plot of ln α vs $1/T$ between 283 and 333 K for methyl lactate: two (*R*)-sensors (open symbols) and two (*S*)-sensors (black symbols).

The enantiomeric purities of all the analytes under investigation could be accurately determined. The resolution power of the applied sensors was astonishingly high: subtle differences of $\Delta\Delta G^0$ values in the range of 15−30 J/mol could be reliably detected at 303 K (5% enantiomeric excess at 285 J/mol, Figure 6). The average error in determining enantiomeric composition was in the range of 1.5−5% at a discrimination factor of $\alpha = 1.12$. With this resolution, it should be possible to discriminate enantiomers with α values as low as 1.01 (or even lower), depending on the vapor pressure of the respective compound and the measuring temperature.

Since the most important feature of such sensors is the possibility to measure "on-line", an immediate practical application in production control, e.g., headspace analysis of the purity of chiral liquids, is conceivable. This holds especially with regard to the industrially important lactates and lactic acid derivatives.

ACKNOWLEDGMENT

We are indebted to the Deutsche Forschungsgemeinschaft (DFG) for financial support in the framework of the "Forschungsschwerpunkt Molekulare Mustererkennung mit Supramolekülen und Polymeren" under Contract No. Go 301/23-1.

Received for review December 30, 1996. Accepted April 9, 1997.[⊗]

AC9612990

[⊗] Abstract published in *Advance ACS Abstracts*, June 1, 1997.